# Optimization of Volumetric Computed Tomography for Skeletal Analysis of Model Genetic Organisms

**SERGIO X. VASQUEZ,[1] MARK S. HANSEN,[2] ALI N. BAHADUR,[1] MATTHEW F. HOCKIN,[3] GORDON L. KINDLMANN,[4] LISA NEVELL,[5] ISABEL Q. WU,[1] DAVID J. GRUNWALD,[3] DAVID M. WEINSTEIN,[4] GREG M. JONES,[4] CHRISTOPHER R. JOHNSON,[4] JOHN L. VANDEBERG,[6] MARIO R. CAPECCHI,[3] AND CHARLES KELLER[1,6,7]***

[1]Greehey Children's Cancer Research Institute, The University of Texas Health Science Center San Antonio, San Antonio, Texas
[2]Department of Pediatrics, University of Utah, Salt Lake City, Utah
[3]Department of Human Genetics, University of Utah, Salt Lake City, Utah
[4]Scientific Computing and Imaging Institute, University of Utah, Salt Lake City, Utah
[5]Center for Advanced Studies in Hominid Paleobiology, The George Washington University, Department of Anthropology, Washington, DC
[6]Southwest Foundation for Biomedical Research, San Antonio, Texas
[7]Department of Cellular & Structural Biology and Department of Pediatrics, The University of Texas Health Science Center San Antonio, San Antonio, Texas

ABSTRACT

Forward and reverse genetics now allow researchers to understand embryonic and postnatal gene function in a broad range of species. Although some genetic mutations cause obvious morphological change, other mutations can be more subtle and, without adequate observation and quantification, might be overlooked. For the increasing number of genetic model organisms examined by the growing field of *phenomics*, standardized but sensitive methods for quantitative analysis need to be incorporated into routine practice to effectively acquire and analyze ever-increasing quantities of phenotypic data. In this study, we present platform-independent parameters for the use of microscopic x-ray computed tomography (microCT) for phenotyping species-specific skeletal morphology of a variety of different genetic model organisms. We show that microCT is suitable for phenotypic characterization for prenatal and postnatal specimens across multiple species. Anat Rec, 291:475–487, 2008. 

**Key words: volumetric x-ray computed tomography; microCT; phenomics; fetus; phenotyping; embryogenesis; imaging; mouse**

The advent of rapid genome sequencing empowers researchers to understand the sequence and structure of genes from multiple species, yet this is only an entry point into the exciting new era of understanding gene function. Intentional genomic modification of model organisms leads to phenotypic variations that reveal the function of the modified gene or gene subset. However, detailed phenotypic analysis is often painstakingly slow, and standardization is only beginning (Brown et al., 2006).

Small animal micro-computed tomography (microCT) is ideally suited to anthropomorphic studies (Turner

The Supplementary Material referred to in this article can be found at http://www.interscience.wiley.com/jpages/1058-8388/suppmat

Grant sponsor: NIH/NCRR Center for Integrative Biomedical Computing; Grant number: P41-RR12553-07.

*Correspondence to: Charles Keller, Greehey Children's Cancer Research Institute, The University of Texas Health Science Center, 8403 Floyd Curl Drive, Mail Code 7784, San Antonio, TX 78229. Fax: 210-562-9014. E-mail: kellerc2@uthscsa.edu

Received 21 September 2007; Accepted 2 January 2008

DOI 10.1002/ar.20670

Published online 19 February 2008 in Wiley InterScience (www.interscience.wiley.com).

et al., 2003; Silha et al., 2003; Moverare et al., 2003) at the macroscopic and microscopic scale, permitting more rapid analysis of certain phenotypes such as skeletal defects and defects of the vasculature system (Paulus et al., 2001; Kindlmann et al., 2005). With the use of metal-containing contrast agents, the fine structure of soft tissues can also be observed and characterized (Johnson et al., 2006). Thus, microCT is a good general performance phenotyping tool.

In this study, we show that microCT is a specifically powerful and practical tool for the skeletal analysis of diverse model genetic organisms. We present guidelines for reproducible, species-specific qualitative and quantitative phenotypic analysis of several genetic model organisms at different stages of development. Species studied include *Mus musculus* (mouse), *Xenopis laevis* (frog), *Danio rerio* (zebrafish), *Myotis lucifugus* (bat), *Monodelphis domestica* (opossum), *Gallus domesticus* (chicken), *Anas domesticus* (duck), and *Microcebus murinus* (mouse lemur). These new guidelines are optimized with respect to the resolution, signal:noise, and artifact reduction that are necessary to detect features of frequent interest for each organism. Investigators may find that, for their specific purposes, slight modification of the settings presented here may be successfully amended to enhance imaging of desired features of interest. Using freely available software for image analysis, we also demonstrate how higher order image processing can enhance the information content of scans.

## MATERIALS AND METHODS

All animals were obtained in accordance with appropriate institutional and governmental animal use guidelines and approvals. MicroCT instruments from two manufacturers were used to scan specimens at settings appropriate for skeletal phenotyping. For scans of 27-μm, 46-μm, and 93-μm resolution (i.e., focal spot width), a GE eXplore Locus in vivo microCT Scanner (GE Healthcare, London, Ontario, Canada) was used. For scans with resolutions ranging from 6 μm to 36 μm, a SCANCO μCT40 specimen scanner (SCANCO USA, Southeastern, PA) was used. Table 1 details the scan parameters for each of the analyzed specimens below.

### Preparation of Mouse Specimens

Newborn and adult *Mus musculus* were euthanized by isoflurane inhalation and staged and scanned using the parameters detailed in Table 1.

### Preparation of Adult Frog

A 15-month-old *Xenopus laevis* specimen was staged and scanned using the parameters detailed in Table 1.

### Preparation of Adult Zebrafish

An adult *Danio rerio* was fixed in 10% buffered formalin, staged, and scanned using the parameters detailed in Table 1.

**TABLE 1. MicroCT scan settings**

| Specimen (common name) | | Scanner | Current (μA) | Voltage (kVp) | Exposure time (msec) | Number of views | Frames per view | Scan time | File size | Scanner resolution setting (focal spot) |
|---|---|---|---|---|---|---|---|---|---|---|
| *Mus musculus* (*mouse*) | newborn | SCANCO μCT40 | 144 | 55 | 300 | 2000 | 5 | 25 hrs | 10GB | 10 μm |
| | adult | GE eXplore Locus | 450 | 80 | 100 | 720 | 5 | 2 hrs | 1.9GB | 93 μm |
| *Xenopis laevis* (frog) | | GE eXplore Locus | 450 | 80 | 100 | 400 | 5 | 20 min | 84MB | 93 μm |
| *Danio rerio* (zebrafish) | | SCANCO μCT40 | 144 | 55 | 300 | 2000 | 10 | 60 hrs | 15GB | 6 μm |
| *Myotis lucifugus* (bat) | adult | GE eXplore Locus | 450 | 80 | 500 | 900 | 10 | 5 hrs | 1.5GB | 46 μm |
| | pelvis and joint | SCANCO μCT40 | 144 | 55 | 300 | 1000 | 5 | 12 hrs | 500MB | 12 μm |
| *Monodelphis domestica* (opossum) | | GE eXplore Locus | 450 | 80 | 100 | 720 | 5 | 5 hrs | 487MB | 93 μm |
| *Gallus domesticus* (chicken) | | SCANCO μCT40 | 144 | 55 | 300 | 2000 | 5 | 22 hrs | 1.5GB | 15 μm |
| *Anas domesticus* (duck) | | SCANCO μCT40 | 144 | 55 | 300 | 1000 | 5 | 18 hrs | 2GB | 36 μm |
| *Microcebus murinus* (mouse lemur) | | GE eXplore Locus | 450 | 80 | 100 | 720 | 5 | 2 hrs | 946MB | 93 μm |

### Preparation of Adult Bat

A 1-year-old adult *Myotis lucifugus* skeleton preparation was staged and scanned using the parameters detailed in Table 1. For skeleton preparations of the bat, abdominal and thoracic organs were removed and carcasses were fixed in 95% ethanol for 4 days. Carcasses were then cleared in 20% glycerol/1% potassium hydroxide for 6 days, transitioned to 50% glycerol/1% potassium hydroxide for 10 days and transferred to 100% glycerol for photography with a digital camera mounted on a dissecting light microscope (Carl Zeiss Stemi 2000 CS, Thornwood, NY).

### Preparation of Adult Opossum

An adult *Monodelphis domestica* was euthanized by $CO_2$ inhalation, staged, and scanned using the parameters detailed in Table 1.

### Preparation of Fetal Chick

White Leghorn chicken eggs (*Gallus domesticus*) were obtained from a regional vendor (Ideal Poultry, Cameron, TX) and incubated in a Lyon R-COM-20 incubator (Lyon Technologies, Inc., Chula Vista, CA) at 38°C and 60% humidity from day 0 to day 14. On day 14, the fetus was harvested and fixed in 10% phosphate buffered saline (PBS) buffered formalin. The fetus was staged and scanned using the parameters detailed in Table 1.

### Preparation of Fetal Duck

White Pekin duck eggs (*Anas domesticus*) were obtained from a national vendor (Duckeggs.com, Chino Hills, CA) and incubated in a Lyon R-COM-20 incubator at 38°C and 60% humidity from day 0 to day 19. On day 19, the fetus was harvested and fixed in 10% PBS buffered formalin. The fetus was staged and scanned using the parameters detailed in Table 1.

### Preparation of Adult Lemur

The eviscerated carcass of a 10-year-old adult lemur (*Microcebus murinus*) was obtained from the Duke University Lemur Center (Durham, NC). The lemur was staged and scanned using the parameters detailed in Table 1.

### Quantitative Analysis

Two-dimensional transfer function (2DTF) visualizations were performed with open source software from the University of Utah Scientific Computing Institute (BioImage, http://www.sci.utah.edu/cibc/software). Data obtained from opossum, mouse, bat, and lemur scans were quantitatively analyzed using open source software with optional bone analysis plug-ins, (MicroView© version 2.1.2, GE Healthcare, http://microview.sourceforge.net) Using this software, right forelimb (humerus, radius) and right hindlimb (femur, tibia) regions of interest were isolated from each specimen scan, then limb lengths were measured using anatomical landmarks at the proximal and distal ends of each bone. Limb length measurements were used to determine the midpoint of the respective shaft. These data were then used to digitally slice a perpendicular cross section of the shaft midpoint. Cortical thickness was taken along three representative areas of this slice and averaged. A $3 \times 3 \times 1$ mm volume of interest (VOI) centered at the midpoint was generated and bone mineral density values were derived from the summed average of this region and from identical regions one millimeter proximal and distal to the midpoint of the shaft.

## RESULTS

### Rapid microCT Scans of Mouse Fetal Skeletons Closely Approximate Data From Traditional Preparations

The mouse has become a mainstay of understanding mammalian gene function and modeling human disease (Kohl et al., 2007; Landstrom et al., 2007; Matera et al., 2007; Tsukumo et al., 2007). An increasing number of studies have taken advantage of microCT for their phenotypic characterizations of adult mouse skeletal morphology (Nieman et al., 2006; Perlyn et al., 2006; Nahrendorf et al., 2007), but fetal skeletal analysis remains challenging (Kindlmann et al., 2004). Nevertheless, accurate methods of analyzing mouse fetuses will be a critical aspect of Tier 1 Phenotyping for the mouse knockout project (Austin et al., 2004).

To determine optimal parameters for mouse fetal skeletal analysis, we performed a series of preliminary scans on fetal mice using a commonly available live animal microCT scanner. We varied specimen medium, x-ray energy, number of views, and frames averaged per view at 27-μm resolution. Results are given in Supplementary Figures S1 and S2, which can be viewed at http://www.interscience.wiley.com/jpages/1058-8388/suppmat. Essentially, a specimen immersed in ethanol at an appropriate x-ray energy (55 kVp) with views at least every 0.5 degrees and multiple averaged frames per view could closely approximate detail given by an alizarin red skeleton preparation. However, the finest features such as the tympanic ring could not be detected, and closely spaced cervical vertebrae could not be resolved from one another. This finding led us to take advantage of a higher resolution microCT specimen scanner whereby similar scan parameters at a higher resolution (10 μm) gave satisfactory results, resolving both the tympanic ring and the cervical vertebrae (Fig. 1). This optimized scan took 25 hr of machine time, but less than 30 min of operator time, which compares favorably to the many hours (or days) required for a traditional alizarin red skeleton preparation.

### Rapid microCT Phenotyping Is Amenable to Adult Xenopus Specimens

*Xenopus laevis*, the African clawed frog, is valued by developmental biologists for the large and easily discernible cell divisions of the egg during embryogenesis. However, morpholino injection techniques have allowed investigators to modify the genome of the frog systematically (Ogino et al., 2006). This advent in genetics is moving analysis beyond the light microscope because a larger field of view is needed to characterize phenotypic changes that may be manifest in adult animals.

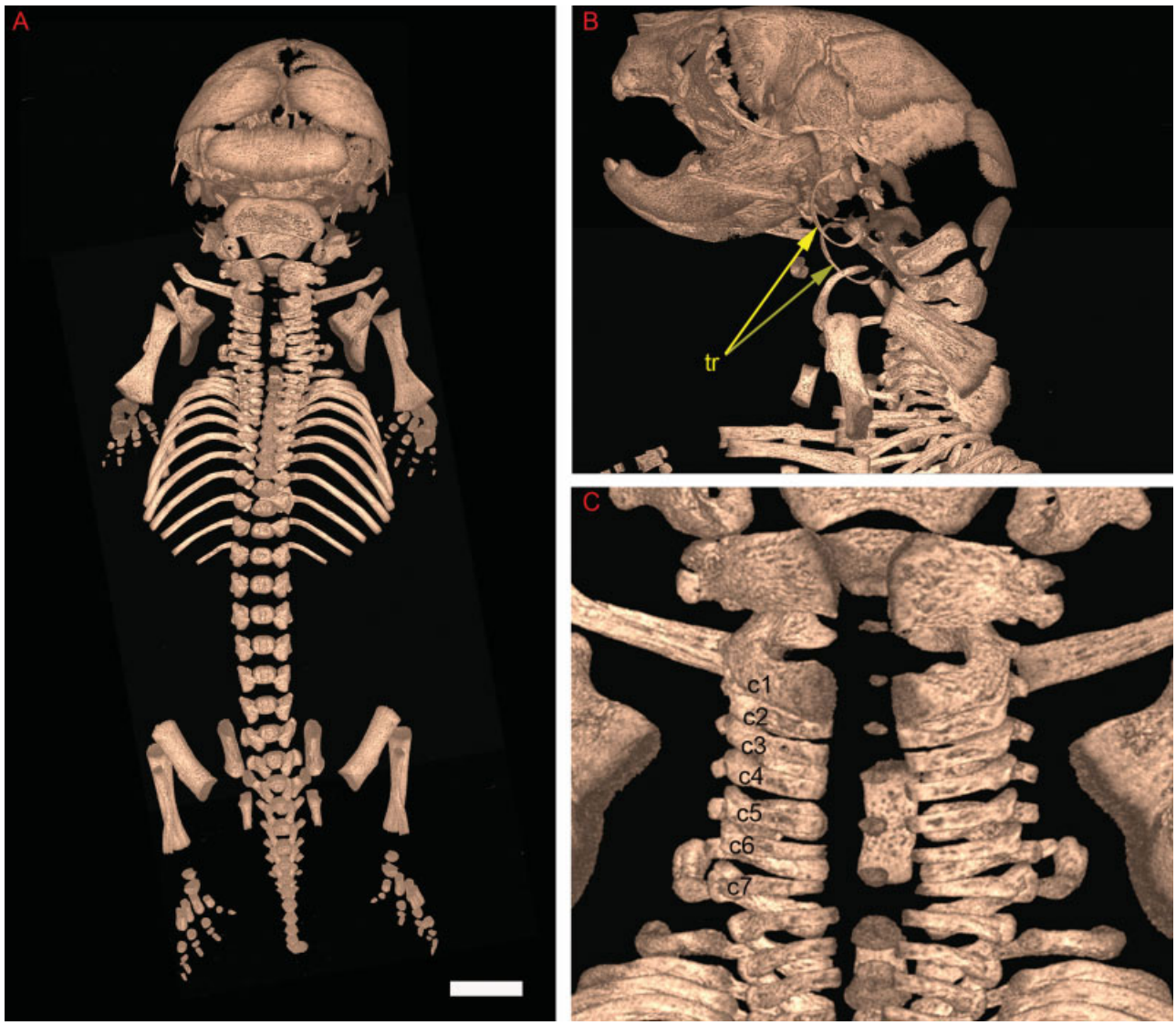


Fig. 1. Traditional and virtual skeletal preparations using a general purpose microCT scanner are similar for the ossified skeleton. Volume rendering of a wild-type postnatal day (P) 0 mouse fetus acquired at 10 μm under optimized parameters. **A:** Dorsal view. **B:** Dorsal close-up of mouse cervical vertebrae. **C:** Close-up of left lateral aspect of mouse skull. Both left and right tympanic rings (tr) are seen in the rendering (yellow arrows). Cervical vertebrae 1–7 are noted (c1–c7). Scale bar = 1.5 mm.

To address the optimized parameters for phenotyping the adult frog, a 93-μm microCT scan was performed on a *Xenopus laevis* specimen. A maximum intensity projection (MIP) is presented in Figure 2A. Regions of higher density are seen as "brighter" than regions of lower density. Digital renderings of the skeleton were generated in different orientations (Fig. 2B–F), and demonstrate that this level of resolution is appropriate to rapidly (within 20 min) phenotype an adult *Xenopus* specimen.

## MicroCT Is a Noninvasive Method of Phenotyping the Very Fine Features of Zebrafish

*Danio rerio*, the teleost zebrafish native to China, has emerged as an important genetic model organism for developmental biology (Dawid, 2004) and human disease (Hsu et al., 2007). Large scale mutagenic screens have been performed (Driever et al., 1996; Geisler et al., 2007) and many stable, heritable, germline mutations have been introduced into inbred colonies for use in embryonic and postembryonic studies. Unfortunately, zebrafish become partially pigmented as adults, which confounds the observation of morphological structures under a light microscope.

To assess the role of microCT in examining the very fine features of adult zebrafish morphology, a 6-μm microCT scan was performed and analyzed using rendering algorithms that are especially well suited to recognize edge boundaries. By using this 2DTF algorithm to generate a rendering (Kindlmann et al., 2005) of the adult zebrafish cranium, one can appreciate in color the discontinuity of zebrafish skull plates as well as overall

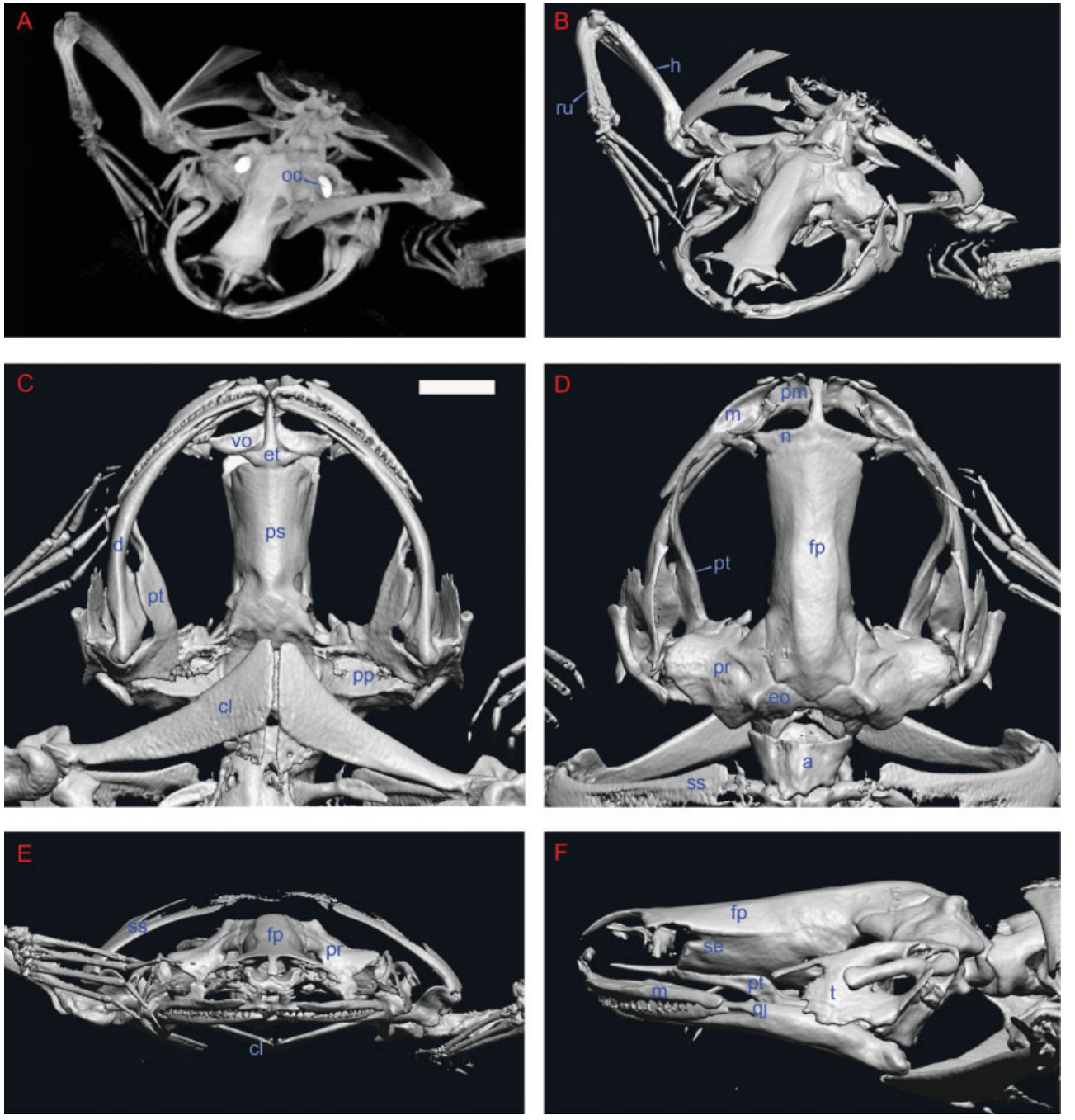


Fig. 2. Nonmammalian genetic model organisms are amenable to phenotyping by microCT. Whole specimen skeletal analysis of African clawed frog, *Xenopus laevis*. **A:** Oblique dorsal maximal intensity projection of a 93-μm focal spot width scan of specimen. Orientation is such that the observer is looking at the frog in a dorsal position, with only the upper third of the specimen in view. The bright, symmetric, electron-dense structures are the otic capsules (oc). **B:** Oblique volume rendering of specimen data in the same orientation as in A. The fused radioulnar (ru) of the frog arm has been demarcated to illustrate this unique skeletal feature of Anurans. **C:** Ventral view. **D:** Dorsal view. The frontoparietal bone (fp) of the skull, also fused in Anurans, is demarcated. **E:** Axial view. **F:** Left lateral view. a, atlas; cl, clavicle; d, dentary; eo, exoccipital; et, ethmoid; h, humerus; m, maxillary; n, nasal; pm, premaxillary; pt, pterygoid; qj, quadratojugal; se, spheneth-moid; ss, suprascapular; t, tympanum; vo, vomer. Scale bar = 3.6 mm.

internal skeletal morphology (Fig. 3A and B, respectively). The Weberian apparatus, a specialized organ for enhancing hearing, is made apparent in the oblique view seen in Figure 3B (white arrow in blue focus circle). Even with a simplified color scheme, the small bony features of the skull are readily apparent (Fig. 3C). In addition to surface morphology, virtual cutaways through the specimen can allow internal structures to be visualized (Fig. 3D). By semitransparent renderings, important internal structures can be

distinguished in their natural orientation deep within the specimen, as is demonstrated by the demarcation of the three pairs of crystalline otoliths residing within the zebrafish inner ear complex (Fig. 3E, light blue). Even the finest structures are delineated in remarkable detail, as shown by the rendered depictions of the isolated zebrafish pectoral fin (Fig. 3F) and the individual segments of the partial zebrafish spine (Fig. 3G).

## Anatomical Landmarks Can Be Identified and Measured Accurately for Comparative Avian Studies Using microCT

In addition to early embryological studies of chick (Kuehnel, 1961; Kurose, 1961; Vigh et al., 1968), current molecular biology techniques and newer imaging technologies have allowed researchers to further investigate limb development (Ohuchi et al., 1998; Saito et al., 2006), bone mineral density (Shahnazari et al., 2006), and beak patterning (Abzhanov et al., 2004; Wu et al., 2006) in the chicken fetus. Because the whole genome of chicken has been sequenced (Wallis et al., 2004), one might reasonably expect that an increase in the numbers of fetal chick phenotyping studies will soon follow (Zhou et al., 2007).

Another avian model of importance, domestic ducks have been used traditionally for the epidemiological characterization of avian influenza (Pantin-Jackwood and Swayne, 2007; Van Borm et al., 2007; Yamamoto et al., 2007), yet their utilization in comparative morphologic studies has been increased in recent years (Wu et al., 2004; Brugmann et al., 2006). In confirmation of the duck's importance as an emerging genetic model organism, a genomic linkage map recently generated from the cross of two Pekin ducks was published to facilitate genomic comparisons between chickens and ducks (Huang et al., 2006).

To determine the utility of microCT for avian fetus studies, we compared overall morphology of the wild-type fetal chick, *Gallus domesticus*, at day 14 of development to that of the wild-type fetal duck, *Anas domesticus*, at day 19 of development. Whole body renderings of chick and duck revealed morphological differences in ovo (Fig. 4A,B). Noticeable in the duck rendering is the scleral ring of the eye (Fig. 4B). Although not seen in the fetal chicken at this particular stage of development, this negative pressure adaptation is believed to be more pronounced in flying and diving birds and is highly variable in the number of plates, thickness, and curvature, dependent upon species (Curtis and Miller, 1938). Comparative meas-

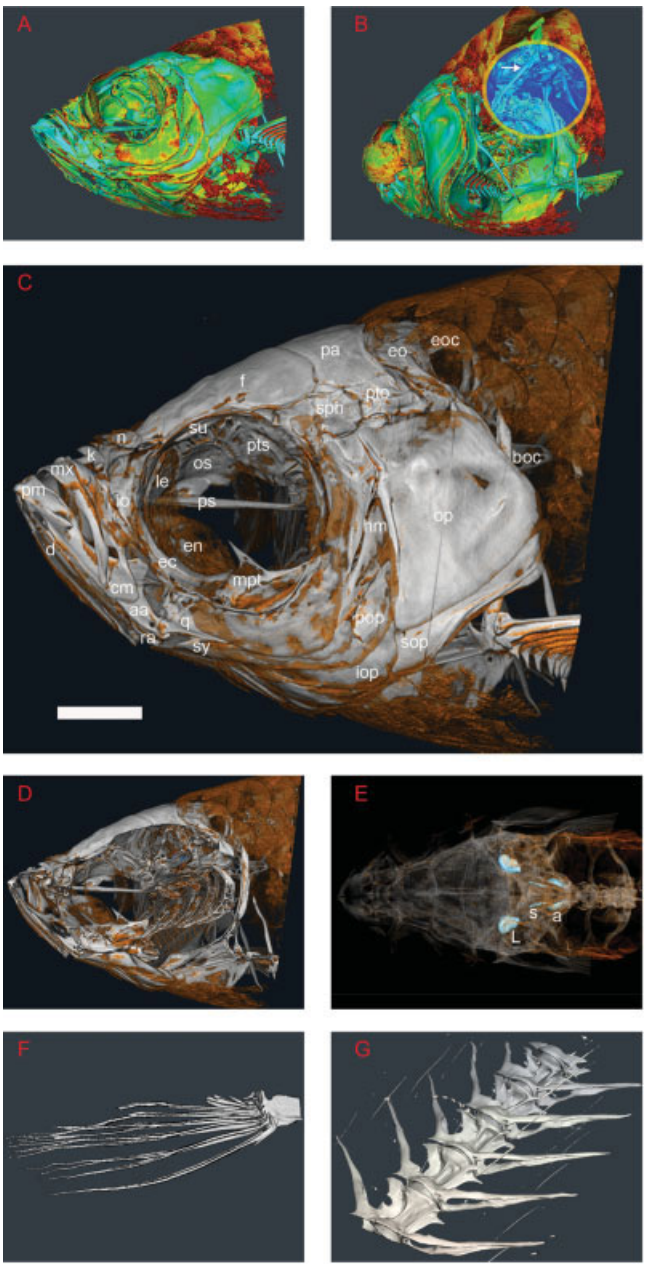


Fig. 3. Advanced rendering algorithms, combined with a higher resolution scanning instrument allow for zebrafish phenotyping. Whole specimen skeletal analysis of adult zebrafish, *Danio rerio*, at 6-μm focal spot width. **A:** Volumetric two-dimensional transfer function rendering of the zebrafish cranium. Renderings such as this left sagittal view of the zebrafish skull help the observer appreciate edge boundaries. **B:** Rendering of zebrafish cranium in the oblique caudal view. The Weberian apparatus, a negative pressure adaptation used in predator detection, is highlighted (white arrow in blue focus ring). **C:** Pseudocolored rendering of the left lateral aspect of the zebrafish skull. **D:** Noninvasive cross-sectional rendering of the zebrafish skull. **E:** Dorsal aspect of the zebrafish, anterior to the left. The bright blue nodules represent the lapillus (L), sagitta (s), and asteriscus (a) (the anterior, medial, and posterior otoliths, respectively) of the adult zebrafish ear. **F:** Rendering of the pectoral fin. The fine structure of the fin bones can be seen despite their inherently small size. **G:** A rendered portion of the ventral aspect of the zebrafish spine showing articulation of individual spinal segments. aa, anguloarticular; boc, basioccipital; cm, coronomeckelian; d, dentary; ec, ectopterygoid; en, entopterygoid; eo, epioccipital; eoc, exoccipital; f, frontal; hm, hyomandibula; io, infraorbital; iop, interopercle; k, kinethmoid; le, lateral ethmoid; mpt, metapterygoid; mx, maxilla; n, nasal; op, opercle; os, orbitosphenoid; pa, parietal; pm, premaxilla; pop, preopercle; ps, parasphenoid; pto, pterotic; pts, pterosphenoid; q, quadrate; ra, retroarticular; soc, supraoccipital; sop, subopercle; sph, sphenotic; su, supraorbital; sy, symplectic. (After Cubbage and Mabee, 1996.) Scale bar = 0.5 mm.

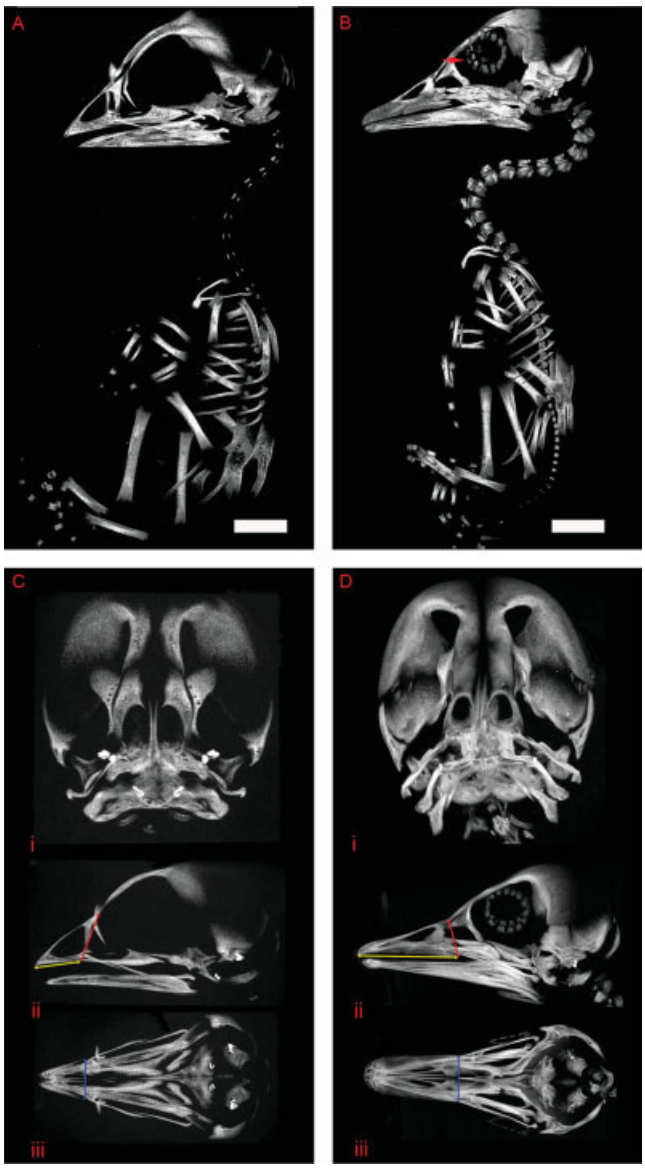


Fig. 4. Anatomical landmarks of avian species can be identified and measured accurately for comparative studies. Whole specimen skeletal analysis of domestic chick at a 30-μm focal spot width and duck at a 36-μm focal spot width. **A:** Rendering of the fetal domestic chicken, *Gallus domesticus*, at embryonic day (E) 14, left lateral view. **B:** Rendering of the fetal domestic duck, *Anas domesticus*, at developmental day E19, left lateral view. Red arrow denotes the scleral ring. **Ci:** A coronal maximum intensity projection (MIP) of the fetal chick skull. **ii:** Left lateral MIP of the fetal chick skull showing beak length (yellow double arrow) and height (red double arrow) landmark measurements. **iii:** Ventral MIP of fetal chick skull showing beak width (blue double arrow) landmark measurement. **Di:** Coronal MIP of the fetal duck skull. **ii:** Left lateral MIP of the fetal duck skull showing beak length (yellow double arrow) and height (red double arrow) measurements. **iii:** Ventral MIP of fetal duck skull showing beak width (blue double arrow) landmark measurement. Scale bar = 4.6 mm in A, 7.0 mm in B.

urements of beak morphology demonstrate differences not only in beak lengths but also their placement relative to the orbits (Fig. 4C,D), which is more distant in the duck.

## Generally Inaccessible Features of the Skeleton Can Be Analyzed Without Destructively Altering Its Natural Position Using microCT Phenotyping Protocols

Bats are the only true flying mammals, yet they comprise one of the largest taxonomic fields in mammalian zoology. *Myotis lucifugus* (otherwise known as the "little brown bat") is one of several bat species currently being characterized as a genetic model organism of great potential, particularly by investigators interested in the genetic basis of bat wing patterning (Lehoczky et al., 2004) and the surprising longevity of particular bat species (Brunet-Rossinni, 2004; Podlutsky et al., 2005).

Although the limbs of a bat are of great interest to comparative biologists, the study of those specimens' bones with articulated joints generally necessitates the disarticulation of bone and socket for further detailed observation. To determine microCT scanner requirements for visualization of gross and fine features of the bat, we used both a live animal scanner and specimen scanner to examine the hip joint and compared our results with traditional light microscopy. Gross light microscope photographs of the pelvis of an eviscerated and cleared adult *Myotis lucifugus* reveal general external features (Fig. 5A), but important features of the femur, such as the greater trochanter (gt), linea aspera (la), and marrow cavity (mc) are not as readily apparent in the photograph as in the 46 μm microCT scan image of the same skeleton preparation (Fig. 5B). A light microscope photograph of the disarticulated femoral head (Fig. 5C) was also surpassed by a specimen scan (12-μm resolution) of the *articulated* femoral head (Fig. 5D). A light microscope picture of the disarticulated bat pelvis (Fig. 5E) was generally comparable to the *articulated* pelvis (12 μm resolution) microCT rendering (Fig. 5F). Thus, microCT scans can perform favorably against traditional skeleton preparations if the scanner resolution is appropriate for the region of interest and disarticulation can be avoided.

## Multi-species Data Can Be Quantitatively Compared Using microCT

The scope of genetic model organisms is continually increasing. *Monodelphis domestica*, the South American gray short-tailed opossum, is the first metatherian mammal to have its genome sequenced (Mikkelsen et al., 2007). Evolutionary (Gallwitz et al., 2006; Belov et al., 2007; Goodstadt et al., 2007) and functional (Ek et al., 2006; Freyer et al., 2007) studies have been extensively conducted, but morphological studies are sparse (Sanchez-Villagra and Maier, 2003; Kitchener et al., 2006). Because of its size similarities to mouse and rat, *Monodelphis domestica* is also emerging as a useful tool for preclinical studies (Chan et al., 2002). Among primates, the mouse lemur *Microcebus murinus* is the smallest of the extant primates and is well known for its utility in the study of aging, both for the physiological (Genin and Perret, 2003; Genin et al., 2003; Cayetanot et al., 2005; Beltran et al., 2007) and psychological effects (Bons et al., 2006; Picq, 2007) that arise at the onset of senescence. With the advent of microCT as an investigative tool for skeletal research, these two species can be further used in comprehensive morphological studies.

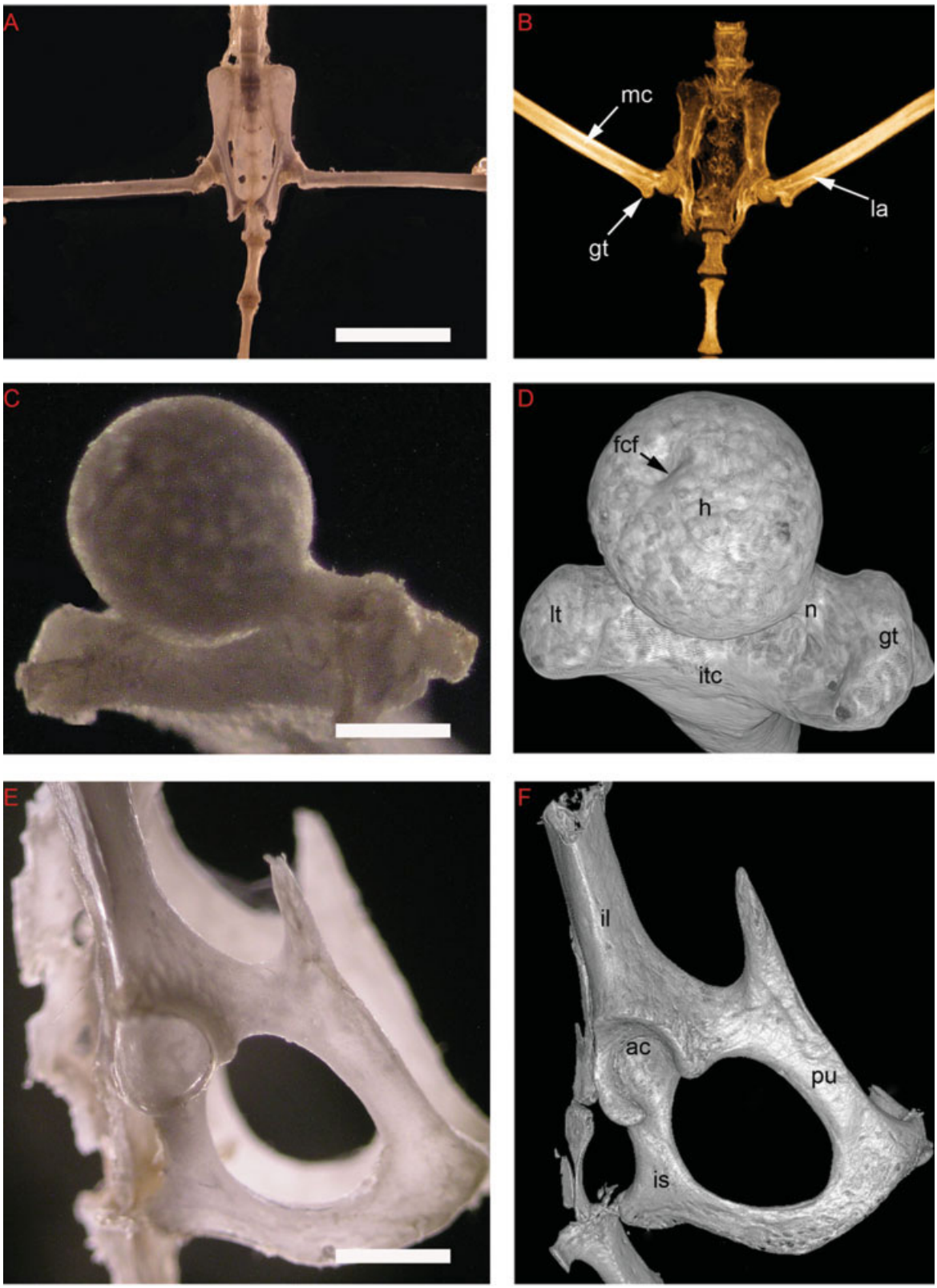


Fig. 5. Morphological areas can be analyzed without destructively altering the natural position of the skeleton. Gross and microCT analysis, pelvis and femur of a skeletal preparation of little brown bat, *Myotis lucifugus*. **A:** Darkfield microscopy of bat pelvis, cleared skeleton preparation. **B:** A maximum intensity projection of 46 μm scan of bat pelvis. Visible are the linea aspire (la), to which muscles attach, and the greater trochanter (gt), a feature of the proximal femur. **C:** Darkfield microscopy of the disarticulated femoral head. **D:** Rendering of 12 μm scan of the *articulated* femoral head (i.e., the scan was cropped, but the specimen bone was intact in the socket during the scan). Pelvis has been cropped out of the image for viewing of femoral features. **E:** Darkfield microscopy of the disarticulated bat pelvis. **F:** Rendering of a 12-μm scan of the *articulated* pelvis. Femur has been cropped out of the image for viewing of pelvic features. ac, acetabulum; fcf, fovea capitis femoris; h, head (of femur); il, ileum; is, ischium; itc, intertrochanteric crest; lt, lesser trochanter; mc, marrow cavity; n, neck (of femur); pu, pubis. Scale bar = 6.0 mm in A, 0.5 mm in C, 2.0 mm in E.

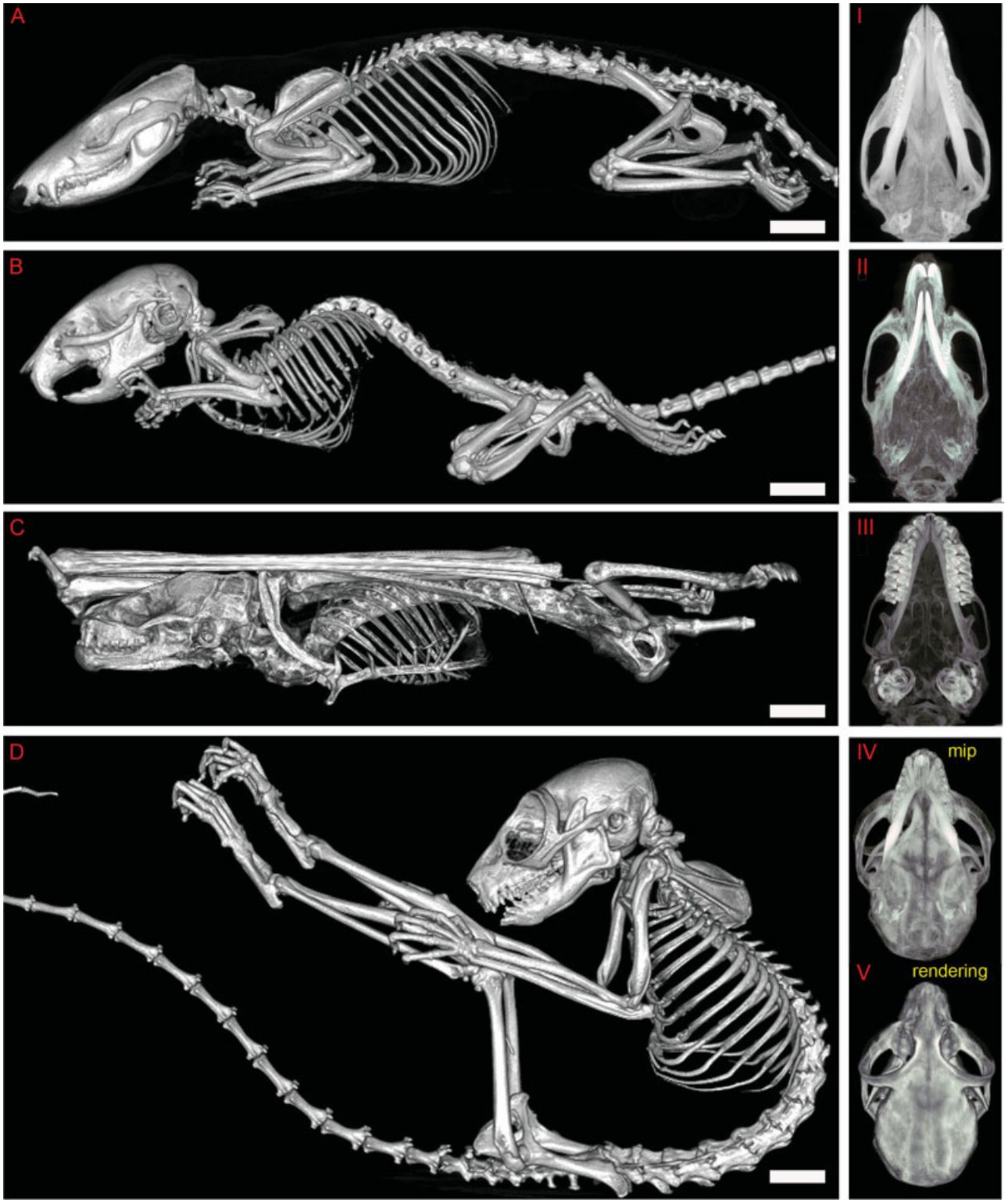


Fig. 6. Multispecies skeletal data can be compared in parallel using microCT. Comparative skeletal data from opossum, mouse, bat, and lemur. **A:** Rendering of *Monodelphis domestica*, the laboratory opossum, a 93-μm focal spot width, whole specimen scan. **I:** A maximum intensity projection (MIP) of the opossum skull. Brightest areas indicate areas of greatest bone density (e.g., teeth, semicircular canals of the inner ear). **B:** A rendering of *Mus musculus*, the laboratory mouse, a 93-μm focal spot width, whole specimen scan. **II:** MIP of the mouse skull. **C:** A rendering of *Myotis lucifugus*, the little brown bat, a 46-μm focal spot width, skeletal preparation. **III:** MIP of the bat skull. **D:** A rendering of *Microcebus murinus*, the mouse lemur, a 93-μm focal spot width, whole specimen scan. **IV:** MIP of the lemur skull. **V:** A rendering of a 93-μm scan of the lemur skull, included for direct comparison between a MIP and a volume rendering. Scale bar = 8.6 mm in A,B, 4.6 mm in C, 8.0 mm in D.

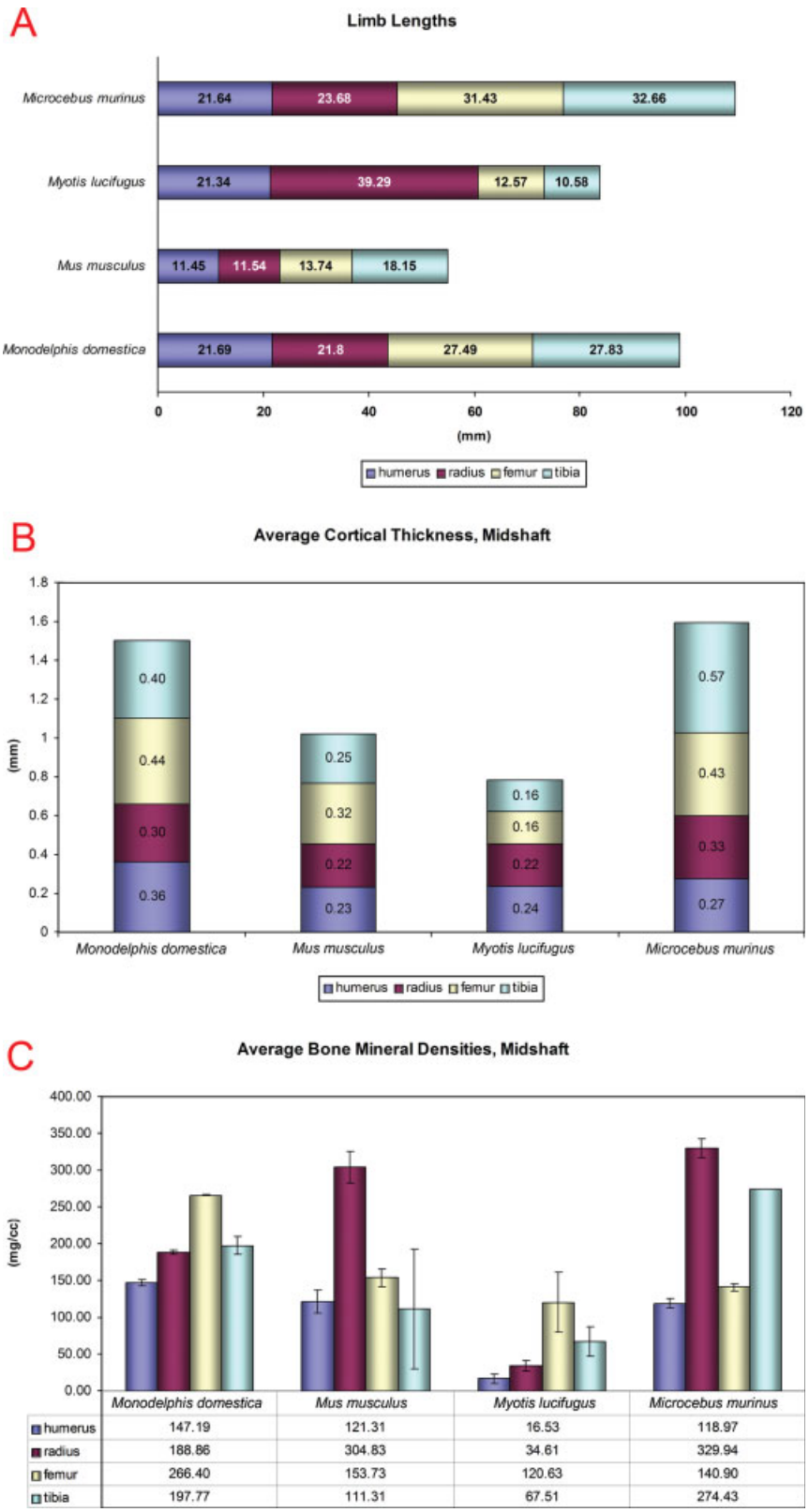


Fig. 7. Quantitative multi-species limb analysis performed using microCT data. **A:** Limb lengths of humerus, radius, femur, and tibia of respective model organisms. Lengths (in mm) are shown at bottom. **B:** Average cortical thickness, midshaft. **C:** Average bone mineral densities, midshaft.

To best exemplify the capabilities of microCT as a general purpose phenotyping tool, a multispecies survey of whole body skeletal morphology was performed for adult *Monodelphis domestica*, *Mus musculus*, *Myotis lucifugus*, and *Microcebus murinus*. All animals were scanned at 93 μm, with the exception of the bat, which was scanned at 46 μm. Sagittal renderings (Figs. A–D) as well as skull MIPs (Fig. 6I–V) were generated for comparison between species. Qualitatively, one can appreciate gross differences among these four specimens including posture, cranial morphology, and dentition adapted to the foraging habits of each model organism. Quantitatively, physical measurements were consistently more precise using microCT scans than using specialized dental calipers (Supplementary Figure S3; standard deviation of humerus length 0.014 mm for microCT vs. 0.84 mm for calipers). The appendicular skeleton of *M. lucifugus* is an outlier because its forelimb length is proportionately longer and its hindlimb length is proportionately shorter (Fig. 7A; humerus:femur ratio 169.8 for *M. lucifugus* vs. 83.3 for *M. musculus*, 78.9 for *M. domestica*, and 68.9 for *M. murinus*). *M. lucifugus* forelimb cortical thickness and bone mineral density (BMD) are also proportionately lower (Fig. 7B,C; averaged stylopod/zeugopod BMD was 25.57 mg/cc for *M. lucifugus* vs. 213.07 mg/cc for *M. musculus*, 168.03 mg/cc for *M. domestica*, and 224.46 mg/cc for *M. murinus*). However, *M. lucifugus* hindlimb cortical thickness and BMD are unexpectedly high compared with its forelimb (averaged stylopod/zeugopod BMD 25.57 mg/cc for upper limbs and 94.07 mg/cc for lower limbs), perhaps as an adaptation to the amount of time spent roosting while not in flight.

## DISCUSSION

Alizarin red and Alcian blue double staining have long been used to visualize bone and cartilage, respectively (Scott and Dorling, 1965; Puchtler et al., 1969). Traditionally, these double stain whole-mount skeleton preparations have been the method of choice for anatomical characterization of assayed mutant skeletons in mutagenic screens, but the protocol is labor intensive and time consuming. MicroCT is emerging as a tool for researchers to acquire digital image data for the ossified skeleton in a fraction of the time, noninvasively and at resolutions equal to or greater than that achievable by direct caliper methods. Indeed, others have successfully used microCT for quantitative biological investigations detailing specific skeletal alterations arising from genetic or physical manipulation (Shanmugarajan et al., 2007; Wang et al., 2007; Sabsovich et al., 2007). In this report, we present platform-independent microCT parameters suitable for analyzing the anatomical features of interest of a variety of genetic model organisms.

We show that microCT is capable of obtaining useful skeletal information similar to that derived from traditional double stain preparations, even for specimens as small as the mouse fetus or adult zebrafish. More accurate visualizations of information content was made possible by optimizing scan parameters (resolution, signal: noise) along with higher order visualization software. Our investigation used several prototypic and emerging genetic model organisms chosen for their utility in a variety of biological studies amenable to skeletal phenotypic characterization. High-resolution imaging was performed non-invasively, a priority characteristic when dealing with cohorts of rare or minute specimens. Most importantly, useful quantitative information was derived for skeletal structures of interest from which inter-species or cross-species analysis can be performed.

Depending upon feature of interest, microCT may be considered a definitive intermediate screening method for phenotyping. A recognized limitation of microCT is the inability to visualize cartilage. Nevertheless, microCT specimens can still be subsequently processed by traditional dual stain skeleton preparations for this purpose (Supplementary Figure S1) Using scanner resolution appropriate to the finest feature of interest is key to successful imaging. A tradeoff exists between spatial resolution and field of view; fortunately, many features of medium to large animals are proportionately larger. However, even with intermediate spatial resolutions, higher order computer algorithms (Kindlmann et al., 2005) can extract sufficient information content to indicate when a sample or subset of samples requires a secondary screen for a selected region of interest. The highest resolution in this report was 6 μm, whereas light microscopes have a spatial resolution of 0.1–0.2 μm; however, commercially available scanners are becoming available at nanoscale resolutions (Brunke et al., 2007), albeit with more limited fields of view. This next generation of submicron imaging is primarily driven by the semiconductor and materials industries (Holzer et al., 2004) yet is predicted to be an available resource for biomedical researchers as well (Larabell and Le Gros, 2004; Frey et al., 2006; Whitesides, 2005; Attwood, 2006).

## ACKNOWLEDGMENTS

We thank Monica Vetter of the University of Utah for providing the *X. laevis* specimen, Janice MacRosin at the Southwest Foundation for Biomedical Research for assistance in acquiring *M. domestica* specimens, and Sarah Zehr of the Duke Lemur center for assistance in acquiring the *M. murinus* specimen. We also appreciate the useful suggestions of Amanda McCleish. Use of SCANCO μCT40 specimen scanner was kindly provided by Numira Biosciences. C.K. is a cofounder and A.N.B. and D.M.W. are employees of Numira Biosciences. This work was made possible in part by software from the NIH/NCRR Center for Integrative Biomedical Computing.

## LITERATURE CITED

Abzhanov A, Protas M, Grant BR, Grant PR, Tabin CJ. 2004. Bmp4 and morphological variation of beaks in Darwin's finches. Science 305:1462–1465.

Attwood D. 2006. Microscopy: nanotomography comes of age. Nature 442:642–643.

Austin CP, Battey JF, Bradley A, Bucan M, Capecchi M, Collins FS, Dove WF, Duyk G, Dymecki S, Eppig JT, Grieder FB, Heintz N, Hicks G, Insel TR, Joyner A, Koller BH, Lloyd KC, Magnuson T, Moore MW, Nagy A, Pollock JD, Roses AD, Sands AT, Seed B, Skarnes WC, Snoddy J, Soriano P, Stewart DJ, Stewart F, Stillman B, Varmus H, Varticovski L, Verma IM, Vogt TF, von Melchner H, Witkowski J, Woychik RP, Wurst W, Yancopoulos GD, Young SG, Zambrowicz B. 2004. The knockout mouse project. Nat Genet 36:921–924.

Belov K, Sanderson CE, Deakin JE, Wong ES, Assange D, McColl KA, Gout A, de Bono B, Barrow AD, Speed TP, Trowsdale J, Papenfuss AT. 2007. Characterization of the opossum immune

genome provides insights into the evolution of the mammalian immune system. Genome Res 17:982–991.
Beltran WA, Vanore M, Ollivet F, Nemoz-Bertholet F, Aujard F, Clerc B, Chahory S. 2007. Ocular findings in two colonies of gray mouse lemurs (Microcebus murinus). Vet Ophthalmol 10:43–49.
Bons N, Rieger F, Prudhomme D, Fisher A, Krause KH. 2006. Microcebus murinus: a useful primate model for human cerebral aging and Alzheimer's disease? Genes Brain Behav 5:120–130.
Brown SD, Hancock JM, Gates H. 2006. Understanding mammalian genetic systems: the challenge of phenotyping in the mouse. PLoS Genet 2:e118.
Brugmann SA, Kim J, Helms JA. 2006. Looking different: understanding diversity in facial form. Am J Med Genet A 140:2521–2529.
Brunet-Rossinni AK. 2004. Reduced free-radical production and extreme longevity in the little brown bat (Myotis lucifugus) vs. two non-flying mammals. Mech Ageing Dev 125:11–20.
Brunke O, Neuber D, Lehmann DK. 2007. NanoCT: visualizing of internal 3D-structures with submicrometer resolution. Mater Res Soc Sym Proc 990.
Cayetanot F, Van Someren EJ, Perret M, Aujard F. 2005. Shortened seasonal photoperiodic cycles accelerate aging of the diurnal and circadian locomotor activity rhythms in a primate. J Biol Rhythms 20:461–469.
Chan J, Robinson ES, Yeh IT, McCarrey JR. 2002. Absence of ras gene mutations in UV-induced malignant melanomas correlates with a dermal origin of melanocytes in Monodelphis domestica. Cancer Lett 184:73–80.
Curtis EL, Miller RC. 1938. The sclerotic ring in north American birds. The Auk 55:225–243.
Dawid IB. 2004. Developmental biology of zebrafish. Ann N Y Acad Sci 1038:88–93.
Driever W, Solnica-Krezel L, Schier AF, Neuhauss SC, Malicki J, Stemple DL, Stainier DY, Zwartkruis F, Abdelilah S, Rangini Z, Belak J, Boggs C. 1996. A genetic screen for mutations affecting embryogenesis in zebrafish. Development 123:37–46.
Ek CJ, Dziegielewska KM, Stolp H, Saunders NR. 2006. Functional effectiveness of the blood-brain barrier to small water-soluble molecules in developing and adult opossum (Monodelphis domestica). J Comp Neurol 496:13–26.
Frey TG, Perkins GA, Ellisman MH. 2006. Electron tomography of membrane-bound cellular organelles. Annu Rev Biophys Biomol Struct 35:199–224.
Freyer C, Zeller U, Renfree MB. 2007. Placental function in two distantly related marsupials. Placenta 28:249–257.
Gallwitz M, Reimer JM, Hellman L. 2006. Expansion of the mast cell chymase locus over the past 200 million years of mammalian evolution. Immunogenetics 58:655–669.
Geisler R, Rauch GJ, Geiger-Rudolph S, Albrecht A, van Bebber F, Berger A, Busch-Nentwich E, Dahm R, Dekens MP, Dooley C, Elli AF, Gehring I, Geiger H, Geisler M, Glaser S, Holley S, Huber M, Kerr A, Kirn A, Knirsch M, Konantz M, Kuchler AM, Maderspacher F, Neuhauss SC, Nicolson T, Ober EA, Praeg E, Ray R, Rentzsch B, Rick JM, Rief E, Schauerte HE, Schepp CP, Schonberger U, Schonthaler HB, Seiler C, Sidi S, Sollner C, Wehner A, Weiler C, Nusslein-Volhard C. 2007. Large-scale mapping of mutations affecting zebrafish development. BMC Genomics 8:11.
Genin F, Perret M. 2003. Daily hypothermia in captive grey mouse lemurs (Microcebus murinus): effects of photoperiod and food restriction. Comp Biochem Physiol B Biochem Mol Biol 136:71–81.
Genin F, Schilling A, Claustrat B. 2003. Melatonin and methimazole mimic short-day-induced fattening in gray mouse lemurs. Physiol Behav 79:553–559.
Goodstadt L, Heger A, Webber C, Ponting CP. 2007. An analysis of the gene complement of a marsupial, Monodelphis domestica: evolution of lineage-specific genes and giant chromosomes. Genome Res 17:969–981.
Holzer L, Indutnyi F, Gasser PH, Munch B, Wegmann M. 2004. Three-dimensional analysis of porous BaTiO3 ceramics using FIB nanotomography. J Microsc 216:84–95.
Hsu CH, Wen ZH, Lin CS, Chakraborty C. 2007. The zebrafish model: use in studying cellular mechanisms for a spectrum of clinical disease entities. Curr Neurovasc Res 4:111–120.
Huang Y, Zhao Y, Haley CS, Hu S, Hao J, Wu C, Li N. 2006. A genetic and cytogenetic map for the duck (Anas platyrhynchos). Genetics 173:287–296.
Johnson JT, Hansen MS, Wu I, Healy LJ, Johnson CR, Jones GM, Capecchi MR, Keller C. 2006. Virtual histology of transgenic mouse embryos for high-throughput phenotyping. PLoS Genet 2:e61.
Kindlmann G, Normann RA, Badi A, Keller C, Jones GM, Johnson CR. 2004. Scientific visualization in small animal imaging. ACM Siggraph Computer Graphics 38:4–7.
Kindlmann GL, Weinstein DM, Jones GM, Johnson CR, Capecchi MR, Keller C. 2005. Practical vessel imaging by computed tomography in live transgenic mouse models for human tumors. Mol Imaging 4:417–424.
Kitchener PD, Hutton EJ, Knott GW. 2006. Primary sensory afferent innervation of the developing superficial dorsal horn in the South American opossum Monodelphis domestica. J Comp Neurol 495:37–52.
Kohl Z, Kandasamy M, Winner B, Aigner R, Gross C, Couillard-Despres S, Bogdahn U, Aigner L, Winkler J. 2007. Physical activity fails to rescue hippocampal neurogenesis deficits in the R6/2 mouse model of Huntington's disease. Brain Res 1155:24–33.
Kuehnel W. 1961. [Morphological and experimental studies on the allantois of chickens.]. Z Zellforsch Mikrosk Anat 54:807–830.
Kurose Y. 1961. The developmental and morphological findings of the anterior chamber angle in chickens. Preliminary results. Nippon Ganka Kiyo 12:771–778.
Landstrom AP, Weisleder N, Batalden KB, Martijn Bos J, Tester DJ, Ommen SR, Wehrens XH, Claycomb WC, Ko JK, Hwang M, Pan Z, Ma J, Ackerman MJ. 2007. Mutations in JPH2-encoded junctophilin-2 associated with hypertrophic cardiomyopathy in humans. J Mol Cell Cardiol 42:1026–1035.
Larabell CA, Le Gros MA. 2004. X-ray tomography generates 3-D reconstructions of the yeast, Saccharomyces cerevisiae, at 60-nm resolution. Mol Biol Cell 15:957–962.
Lehoczky JA, Williams ME, Innis JW. 2004. Conserved expression domains for genes upstream and within the HoxA and HoxD clusters suggests a long-range enhancer existed before cluster duplication. Evol Dev 6:423–430.
Matera I, Cockroft JL, Moran JL, Beier DR, Goldowitz D, Pavan WJ. 2007. A mouse model of Waardenburg syndrome type IV resulting from an ENU-induced mutation in endothelin 3. Pigment Cell Res 20:210–215.
Mikkelsen TS, Wakefield MJ, Aken B, Amemiya CT, Chang JL, Duke S, Garber M, Gentles AJ, Goodstadt L, Heger A, Jurka J, Kamal M, Mauceli E, Searle SM, Sharpe T, Baker ML, Batzer MA, Benos PV, Belov K, Clamp M, Cook A, Cuff J, Das R, Davidow L, Deakin JE, Fazzari MJ, Glass JL, Grabherr M, Greally JM, Gu W, Hore TA, Huttley GA, Kleber M, Jirtle RL, Koina E, Lee JT, Mahony S, Marra MA, Miller RD, Nicholls RD, Oda M, Papenfuss AT, Parra ZE, Pollock DD, Ray DA, Schein JE, Speed TP, Thompson K, VandeBerg JL, Wade CM, Walker JA, Waters PD, Webber C, Weidman JR, Xie X, Zody MC, Baldwin J, Abdouelleil A, Abdulkadir J, Abebe A, Abera B, Abreu J, Acer SC, Aftuck L, Alexander A, An P, Anderson E, Anderson S, Arachi H, Azer M, Bachantsang P, Barry A, Bayul T, Berlin A, Bessette D, Bloom T, Bloom T, Boguslavskiy L, Bonnet C, Boukhgalter B, Bourzgui I, Brown A, Cahill P, Channer S, Cheshatsang Y, Chuda L, Citroen M, Collymore A, Cooke P, Costello M, D'Aco K, Daza R, De Haan G, DeGray S, DeMaso C, Dhargay N, Dooley K, Dooley E, Doricent M, Dorje P, Dorjee K, Dupes A, Elong R, Falk J, Farina A, Faro S, Ferguson D, Fisher S, Foley CD, Franke A, Friedrich D, Gadbois L, Gearin G, Gearin CR, Giannoukos G, Goode T, Graham J, Grandbois E, Grewal S, Gyaltsen K, Hafez N, Hagos B, Hall J, Henson C, Hollinger A, Honan T, Huard MD, Hughes L, Hurhula B, Husby ME, Kamat A, Kanga B, Kashin S, Khazanovich D, Kisner P, Lance K, Lara M, Lee W, Lennon N, Letendre F, LeVine R, Lipovsky A, Liu X, Liu J, Liu S, Lokyitsang T, Lokyitsang Y, Lubonja R, Lui A, MacDonald P, Magnisalis

V, Maru K, Matthews C, McCusker W, McDonough S, Mehta T, Meldrim J, Meneus L, Mihai O, Mihalev A, Mihova T, Mittelman R, Mlenga V, Montmayeur A, Mulrain L, Navidi A, Naylor J, Negash T, Nguyen T, Nguyen N, Nicol R, Norbu C, Norbu N, Novod N, O'Neill B, Osman S, Markiewicz E, Oyono OL, Patti C, Phunkhang P, Pierre F, Priest M, Raghuraman S, Rege F, Reyes R, Rise C, Rogov P, Ross K, Ryan E, Settipalli S, Shea T, Sherpa N, Shi L, Shih D, Sparrow T, Spaulding J, Stalker J, Stange-Thomann N, Stavropoulos S, Stone C, Strader C, Tesfaye S, Thomson T, Thoulutsang Y, Thoulutsang D, Topham K, Topping I, Tsamla T, Vassiliev H, Vo A, Wangchuk T, Wangdi T, Weiand M, Wilkinson J, Wilson A, Yadav S, Young G, Yu Q, Zembek L, Zhong D, Zimmer A, Zwirko Z, Jaffe DB, Alvarez P, Brockman W, Butler J, Chin C, Gnerre S, MacCallum I, Graves JA, Ponting CP, Breen M, Samollow PB, Lander ES, Lindblad-Toh K. 2007. Genome of the marsupial Monodelphis domestica reveals innovation in noncoding sequences. Nature 447:167–177.

Moverare S, Venken K, Eriksson AL, Andersson N, Skrtic S, Wergedal J, Mohan S, Salmon P, Bouillon R, Gustafsson JA, Vanderschueren D, Ohlsson C. 2003. Differential effects on bone of estrogen receptor alpha and androgen receptor activation in orchidectomized adult male mice. Proc Natl Acad Sci U S A 100:13573–13578.

Nahrendorf M, Badea C, Hedlund LW, Figueiredo JL, Sosnovik DE, Johnson GA, Weissleder R. 2007. High resolution imaging of murine myocardial infarction with delayed enhancement cine micro-CT. Am J Physiol Heart Circ Physiol 292:H3172–H318.

Nieman BJ, Flenniken AM, Adamson SL, Henkelman RM, Sled JG. 2006. Anatomical phenotyping in the brain and skull of a mutant mouse by magnetic resonance imaging and computed tomography. Physiol Genomics 24:154–162.

Ogino H, McConnell WB, Grainger RM. 2006. High-throughput transgenesis in Xenopus using I-SceI meganuclease. Nat Protoc 1:1703–1710.

Ohuchi H, Takeuchi J, Yoshioka H, Ishimaru Y, Ogura K, Takahashi N, Ogura T, Noji S. 1998. Correlation of wing-leg identity in ectopic FGF-induced chimeric limbs with the differential expression of chick Tbx5 and Tbx4. Development 125:51–60.

Pantin-Jackwood MJ, Swayne DE. 2007. Pathobiology of Asian highly pathogenic avian influenza H5N1 virus infections in ducks. Avian Dis 51:250–259.

Paulus MJ, Gleason SS, Easterly ME, Foltz CJ. 2001. A review of high-resolution X-ray computed tomography and other imaging modalities for small animal research. Lab Anim (NY) 30:36–45.

Perlyn CA, DeLeon VB, Babbs C, Govier D, Burell L, Darvann T, Kreiborg S, Morriss-Kay G. 2006. The craniofacial phenotype of the Crouzon mouse: analysis of a model for syndromic craniosynostosis using three-dimensional MicroCT. Cleft Palate Craniofac J 43:740–748.

Picq JL. 2007. Aging affects executive functions and memory in mouse lemur primates. Exp Gerontol 42:223–232.

Podlutsky AJ, Khritankov AM, Ovodov ND, Austad SN. 2005. A new field record for bat longevity. J Gerontol A Biol Sci Med Sci 60:1366–1368.

Puchtler H, Meloan SN, Terry MS. 1969. On the history and mechanism of alizarin and alizarin red S stains for calcium. J Histochem Cytochem 17:110–124.

Sabsovich I, Clark JD, Liao G, Peltz G, Lindsey DP, Jacobs CR, Yao W, Guo TZ, Kingery WS. 2007. Bone microstructure and its associated genetic variability in 12 inbred mouse strains: muCT study and in silico genome scan. Bone 42:439–451.

Saito D, Yonei-Tamura S, Takahashi Y, Tamura K. 2006. Level-specific role of paraxial mesoderm in regulation of Tbx5/Tbx4 expression and limb initiation. Dev Biol 292:79–89.

Sanchez-Villagra MR, Maier W. 2003. Ontogenesis of the scapula in marsupial mammals, with special emphasis on perinatal stages of didelphids and remarks on the origin of the therian scapula. J Morphol 258:115–129.

Scott JE, Dorling J. 1965. Differential staining of acid glycosaminoglycans (mucopolysaccharides) by alcian blue in salt solutions. Histochemie 5:221–233.

Shahnazari M, Sharkey NA, Fosmire GJ, Leach RM. 2006. Effects of strontium on bone strength, density, volume, and microarchitecture in laying hens. J Bone Miner Res 21:1696–1703.

Shanmugarajan S, Irie K, Musselwhite C, Key L Jr, Ries W, Reddy S. 2007. Transgenic mice with OIP-1/hSca overexpression targeted to the osteoclast lineage develop an osteopetrosis bone phenotype. J Pathol 213:420–428.

Silha JV, Mishra S, Rosen CJ, Beamer WG, Turner RT, Powell DR, Murphy LJ. 2003. Perturbations in bone formation and resorption in insulin-like growth factor binding protein-3 transgenic mice. J Bone Miner Res 18:1834–1841.

Tsukumo DM, Carvalho-Filho MA, Carvalheira JB, Prada PO, Hirabara SM, Schenka AA, Araujo EP, Vassalo J, Curi R, Velloso LA, Saad MJ. 2007. Loss-of-function mutation in TLR4 prevents diet-induced obesity and insulin resistance. Diabetes 56:1986–1998.

Turner CH, Sun Q, Schriefer J, Pitner N, Price R, Bouxsein ML, Rosen CJ, Donahue LR, Shultz KL, Beamer WG. 2003. Congenic mice reveal sex-specific genetic regulation of femoral structure and strength. Calcif Tissue Int 73:297–303.

Van Borm S, Steensels M, Ferreira HL, Boschmans M, De Vriese J, Lambrecht B, van den Berg T. 2007. A universal avian endogenous real-time reverse transcriptase-polymerase chain reaction control and its application to avian influenza diagnosis and quantification. Avian Dis 51:213–220.

Vigh B, Tar E, Teichmann I. 1968. The development of the paraventricular organ in the white Leghorn chicken. Acta Biol Acad Sci Hung 19:215–225.

Wallis JW, Aerts J, Groenen MA, Crooijmans RP, Layman D, Graves TA, Scheer DE, Kremitzki C, Fedele MJ, Mudd NK, Cardenas M, Higginbotham J, Carter J, McGrane R, Gaige T, Mead K, Walker J, Albracht D, Davito J, Yang SP, Leong S, Chinwalla A, Sekhon M, Wylie K, Dodgson J, Romanov MN, Cheng H, de Jong PJ, Osoegawa K, Nefedov M, Zhang H, McPherson JD, Krzywinski M, Schein J, Hillier L, Mardis ER, Wilson RK, Warren WC. 2004. A physical map of the chicken genome. Nature 432:761–764.

Wang Y, Wan C, Szoke G, Ryaby JT, Li G. 2007. Local injection of thrombin-related peptide (TP508) in PPF/PLGA microparticles-enhanced bone formation during distraction osteogenesis. J Orthop Res [Epub ahead of print].

Whitesides GM. 2005. Nanoscience, nanotechnology, and chemistry. Small 1:172–179.

Wu P, Jiang TX, Shen JY, Widelitz RB, Chuong CM. 2006. Morphoregulation of avian beaks: comparative mapping of growth zone activities and morphological evolution. Dev Dyn 235:1400–1412.

Wu P, Jiang TX, Suksaweang S, Widelitz RB, Chuong CM. 2004. Molecular shaping of the beak. Science 305:1465–1466.

Yamamoto Y, Nakamura K, Kitagawa K, Ikenaga N, Yamada M, Mase M, Narita M. 2007. Severe nonpurulent encephalitis with mortality and feather lesions in call ducks (Anas platyrhyncha var. domestica) inoculated intravenously with H5N1 highly pathogenic avian influenza virus. Avian Dis 51:52–57.

Zhou H, Deeb N, Evock-Clover CM, Mitchell AD, Ashwell CM, Lamont SJ. 2007. Genome-wide linkage analysis to identify chromosomal regions affecting phenotypic traits in the chicken. III. Skeletal integrity. Poult Sci 86:255–266.